Numerical simulation of TIG welding arc using LSFEM method for the magnetic induction computation

Michel Brochard, Stephane Gounand, Marc Medale

Numerical simulation of TIG welding arc using LSFEM method for the magnetic field computation

Brochard, M. [1], Gounand, S.[2], Médale, M. [3]

[1] CEA Saclay, DEN/DANS/DM2S/SEMT/LTA, bâtiment 611, 91191 Gif-Sur-Yvette Cedex, France
[2] CEA Saclay, DEN/DANS/DM2S/SFME/LTMF, bâtiment 454, 91191 Gif-Sur-Yvette Cedex, France
[3] École Polytech' Marseille, IUSTI, 5, rue Enrico Fermi, 13453 Marseille Cedex
Email : michel.brochard@cea.fr

Keywords: TIG welding, arc plasma, LSFEM method, numerical simulation

Abstract

A two-dimensional axisymmetric arc model has been developed to describe heat and mass transfers. It is applied to a tungsten cathode, an argon plasma, and a copper anode. In order to efficiently calculate the magnetic flux density vector, and hence the electromagnetic contributions involved, the Least Square Finite Element Method is used (LSFEM). It gives many benefits : the magnetic flux density vector is directly computed and this method can be easily extended to three-dimensional geometries. Besides, it permits not to make a commonly used oversimplification by imposing a hypothesis on the current density when the magnetostatic problem is solved. Results show that making this assumption slightly modifies the temperature, magnetic field and velocity distributions in the whole domain.

1. Introduction

In many industrial joining problems the assembly quality is related to the weld quality. In order to minimize undesirable mechanical effects (residual stresses, assembly distortions), numerical modelling can be used. But the pertinence of the results is strongly dependent on the boundary conditions description such as, for example, the heat source transferred to the workpiece. A promising way to define the source properly is to make a good description of the physical phenomena involved in the mass, momentum, and energy balances in the arc and weld pool.

In tungsten inert gas (TIG) welding, an electric arc is generated between the electrode and the workpiece, where electromagnetic interactions (Lorentz force, Joule heating) and several heat transfer modes (diffusion, advection, radiation…) are involved (figure 1).

Many arc models have been developed since the first description of the entire high-intensity free-burning arc was published [1]. In this model, the physics of a steady and rotationally symmetric free-burning high-intensity argon arc was well described. Since then, it is often used as a benchmark for codes before improving them by introducing more realistic physics. For instance, studies have been done on a three dimensional arc model with metal vapours [2] or, taking account of departures from equilibrium in the electrode sheath regions [3].

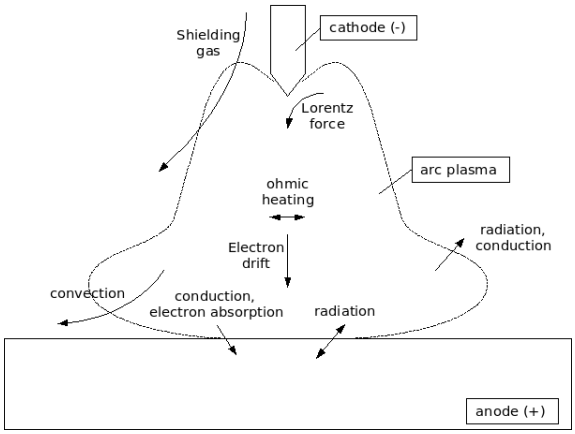

Figure 1: Physical phenomena in TIG arc welding

Also, understanding weld pool phenomena is necessary to predict the weld quality. In this way, many weld pools models [4] have been published.

More recently, numerical models have been made to describe a unified arc and weld pool model [5]. Lately, Hirata and al. [6] established an improved numerical model which takes in account the metal transfer to describe gas shielded metal arc welding processes. However, in these models, Lorentz forces are generally not well estimated because of hypotheses or chosen methods.

The purpose of this paper is to present the Least Square Finite Element method to efficiently compute the magnetic flux density vector, and hence the several electromagnetic contributions in a welding arc. The benefit of this method will be explained. A numerical model of TIG arc welding with cooled copper anode and tungsten cathode has been developed in order to describe heat transfer, mass, and fluid flow in the arc plasma.

2. Mathematical model

2.1 Assumptions

The arc model contains the following assumptions:

- The arc plasma is described as a fluid at atmospheric pressure in two-dimensional axisymmetric coordinate.
- The flow is laminar and quasi-incompressible since the Mach number is small in the arc column (the sound velocity of pure argon is close to 2500 $m.s^{-1}$ at 10000 K). And hence, we assume that compressibility effects are negligible. Therefore, physical and thermodynamic properties are supposed to be only dependent on the local temperature.
- The arc plasma is in pure argon in Local Thermodynamic Equilibrium (LTE).
- Cathode and anode surfaces are considered to be spatially and temporally not deformable.

- A steady state solution is assumed to exist.

2.2 Governing equations

2.2.1. Plasma modelling

The governing conservation equations are:

- the mass conservation equation:

$$\nabla\cdot(\rho\boldsymbol{u})=0 \tag{1}$$

- the momentum conservation equation:

$$\rho\boldsymbol{u}\nabla\boldsymbol{u}+\nabla P-\nabla\cdot\bar{\bar{\tau}}=\boldsymbol{J}\times\boldsymbol{B} \tag{2}$$

with the rate-of-strain tensor $\bar{\bar{\tau}}$ defined by : $\bar{\bar{\tau}}=\mu\left[(\nabla\boldsymbol{u})\cdot(\nabla\boldsymbol{u})^{T}-\frac{2}{3}(\nabla\cdot\boldsymbol{u})\bar{\bar{I}}\right]$

where $\bar{\bar{I}}$ is the identity matrix.

- the energy conservation equation:

$$\rho C_p\boldsymbol{u}\nabla T-\nabla\cdot(\lambda\nabla T)=\frac{\|\boldsymbol{J}\|^2}{\sigma}+\frac{5k_b}{2e}\boldsymbol{J}\cdot\nabla T-4\pi\varepsilon_N \tag{3}$$

where P is the dynamic pressure, **u** the velocity, T the temperature, **J** the current density, and **B** the magnetic flux density vector. The transport and thermodynamic coefficients, considered to be only a function of the local temperature, are the density ρ, the viscosity μ, the thermal conductivity λ, the specific heat Cp, and the net emission coefficient ε_N. These physical properties values are taken from [7] and [2]. Besides, k_b is the Boltzmann constant and e the electron charge.

The term on the right side of the momentum conservation equation represents the Lorentz force. The first term on the right side of the energy conservation equation corresponds to the ohmic heating, and the second term, to the electronic enthalpic flux. The last term describes the radiation losses .

In order to define the electromagnetic source terms we have to solve an electromagnetic model (equations (4), (5), (6), (7)), which is based on the Maxwell equations in quasi-steady state and in pure diffusion, due to small magnetic Reynolds ($R_{em} = \mu_0 L_0 \sigma_0 U_0 \sim 0{,}01$ [8]).

$$\nabla\cdot\boldsymbol{J}=0 \tag{4}$$

$$\boldsymbol{J}=-\sigma\nabla\phi \tag{5}$$

$$\nabla\times\boldsymbol{B}=\mu_0\boldsymbol{J} \tag{6}$$

$$\nabla\cdot\boldsymbol{B}=0 \tag{7}$$

where μ_0 is the magnetic permeability of vacuum and ϕ the electric potential.

This model can be separated in two (models (8) and (9)). First, we solve ϕ to calculate the current density **J**. Next, the magnetostatic problem is solved to find the magnetic flux density vector **B**.

$$\begin{gathered}\nabla\cdot(-\sigma\nabla\phi)=0 \ \ on \ \ \Omega,\ \phi=\phi_{imp} \ \ on \ \ \partial\Omega_1,\\ -\sigma\nabla\phi\cdot\boldsymbol{n}=\boldsymbol{J}_{\boldsymbol{imp}}\cdot\boldsymbol{n} \ \ on \ \ \partial\Omega_2\end{gathered} \tag{8}$$

$$\begin{gathered}\nabla\times\boldsymbol{B}=\mu_0\boldsymbol{J}_{\boldsymbol{imp}} \ \ on \ \ \Omega,\ \nabla\cdot\boldsymbol{B}=0 \ \ on\Omega,\\ \boldsymbol{n}\cdot\boldsymbol{B}=0 \ \ on \ \ \partial\Omega_3,\ \boldsymbol{n}\times\boldsymbol{B}=\boldsymbol{0} \ \ on \ \ \partial\Omega_4\end{gathered} \tag{9}$$

where Ω is the domain volume, and $\partial\Omega_i$ are the boundary interfaces i.

Because (9) is a first order system, it leads to difficulties when solving by classical Galerkin method [9]. To obtain the azimuthal **B** field, most authors use only Ampere's law (6), assuming that most of the current can be represented by the axial component of **J** :

$$B_\theta=\frac{\mu_0}{r}\int_0^R j_z r\,dr \tag{10}$$

where r and z are respectively the radial and axial coordinates, and R the domain radius.

Unfortunately, this method is not adapted to three-dimensional problems because of this hypothesis and, because Gauss' law (7) is not included in the calculation.

Some authors [2] recast (9) into a second order system (12) introducing a vector potential **A** (equation (11)) in equation (6). To ensure the uniqueness of the solution, a condition on its divergence $(\nabla\cdot\boldsymbol{A}=0)$, called the gauge condition, has to be imposed.

$$\boldsymbol{B}=\nabla\times\boldsymbol{A} \tag{11}$$

$$\nabla^2\boldsymbol{A}=-\mu_0\boldsymbol{J} \tag{12}$$

Nevertheless, the introduction of this magnetostatic vector potential **A** does not bring much benefit at all because in one hand, **B** field is computed after two steps, and in another hand it is not so easy to find suitable boundary conditions for **A**.

In order to avoid these disadvantages, in this paper, the magnetostatic part is worked out with the Least Square Finite Element Method (LSFEM) [10] that leads to solve the following equation:

$$\int_\Omega\left[(\nabla\times\boldsymbol{B})\cdot(\nabla\times\boldsymbol{B}')\right]d\Omega+\int_\Omega\left[(\nabla\cdot\boldsymbol{B})\cdot(\nabla\cdot\boldsymbol{B}')\right]d\Omega=\int_\Omega\left[\mu_0\boldsymbol{J}_{\boldsymbol{imp}}\cdot(\nabla\times\boldsymbol{B}')\right]d\Omega \tag{13}$$

where **B'**, the weighting function, has the same differential operator as that of trial function **B**.

This formulation gives many advantages:

- The divergence of **B** is easily included.
- It can be applied in several geometries even for three-dimensional problems.
- It gives a symmetric, positive definite system that can be solved easily with iterative solver.

2.2.2.Anode and cathode modelling

Because the melting temperature is not reached in the cooled anode and cathode parts, we solve only the energy conservation equation (14) and the electromagnetic model (equations (8) and (9)) in these domains.

$$\nabla\cdot(-\lambda\nabla T)=\frac{\|\boldsymbol{J}\|^2}{\sigma} \tag{14}$$

The physical properties of pure tungsten for the cathode, and, pure copper for the anode, are temperature dependent andare taken from tables [11].

2.2.3.Auxiliary equations

In order to maintain energy conservation at electrode interfaces, we use the following relations ([2], [8]):

$$\left[-\lambda\left(\frac{\partial T}{\partial z}\right)\right]_{anode}-\left[-\lambda\left(\frac{\partial T}{\partial z}\right)\right]_{plasma}=\|\boldsymbol{J}\|\left(V_a+\Phi_S\right)-\sigma_B\,\varepsilon\,T^4 \tag{15}$$

$$\left[-\lambda\left(\frac{\partial T}{\partial n}\right)\right]_{plasma}-\left[-\lambda\left(\frac{\partial T}{\partial n}\right)\right]_{cathode}=\|\boldsymbol{J}\|V_c-\sigma_B\,\varepsilon\,T^4 \tag{16}$$

where V_a and V_c are respectively the anode and cathode fall voltages (3.5 and 3 V), Φ_S (4.65 V) the anode work function [2], σ_B the Stefan-Boltzmann constant, ε the emissivity. Due to the anode and cathode fall voltages at the electrode, condensation of electrons at the anode surface and radiation, source terms are added at the interface balance equations (15) and (16).

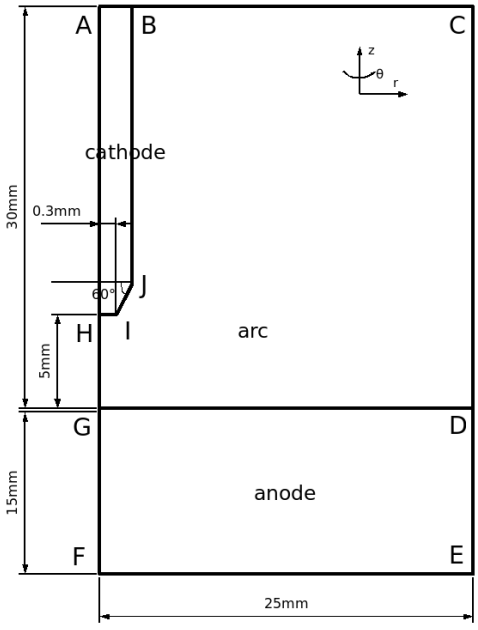

Figure 2: Free-burning arc geometry

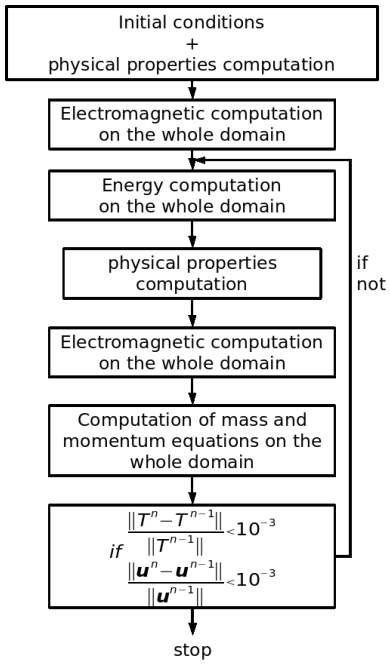

Figure 3: Computational procedure

	AB	GH	CD	DE	EF	FG	BC	HA	GD	HI, IJ, JB
u_r		$u_r=0$	$\boldsymbol{n}\cdot\bar{\bar{\tau}}\cdot\boldsymbol{n}=\boldsymbol{0}$				$\boldsymbol{n}\,\bar{\bar{\tau}}\cdot\boldsymbol{n}=\boldsymbol{0}$		$u_r=0$	$u_r=0$
u_z			and $u_z=0$				and $u_r=0$		$u_z=0$	$u_z=0$
T	$T=300\,K$	$\frac{\partial T}{\partial r}=0$	$T=300\,K$	$T=300\,K$	$T=300\,K$	$\frac{\partial T}{\partial r}=0$	$T=300\,K$	$\frac{\partial T}{\partial r}=0$	eq. (15)	eq. (16)
ϕ	$-\sigma\frac{\partial \phi}{\partial z}=J_c$ $J_c=\frac{I}{\pi R_c^2}$	$\frac{\partial \phi}{\partial r}=0$	$\frac{\partial \phi}{\partial r}=0$	$\frac{\partial \phi}{\partial r}=0$	$\phi=0$	$\frac{\partial \phi}{\partial r}=0$	$\frac{\partial \phi}{\partial z}=0$	$\frac{\partial \phi}{\partial r}=0$		
B_θ		$B_\theta=0$				$B_\theta=0$		$B_\theta=0$		

Table 1: Boundary conditions

2.2.1.Calculation domain and boundary conditions

In order to study the energy, mass and fluid flow transfers in the whole domain, we choose a free-burning arc geometry commonly used in [5]. Dimensions are given in figure 2.

The numerical domain includes a tungsten cathode with a 60° angle tip, a copper anode and a plasma column in pure argon at atmospheric pressure. The current intensity varies between 100 and 150 A and the inter-electrode distance is kept constant at 5 mm.

The boundary conditions are indicated in table 1. At the top of the cathode, we impose a constant current density Jc which depends on the cathode radius R_c and on the total current I. We consider the outer boundaries to be at ambient temperature and the arc domain to be opened.

2.2.2.Discretization and numerical procedure

The calculation domain is represented by a grid of 5228 finite elements composed of linear elements Q1 for the pressure and quadratic elements Q2 for all the other variables. The mesh is refined near the axial discharge axis and on the electrode interfaces.

Classical Galerkin formulation [9] is used for all the computed equations, except for the **B** calculation, where the LSFEM formulation is employed (13). The discrete non linear problem is worked out by a Newton-Raphson algorithm and by the calculation procedure presented in figure 3.

The space discretization and the computation of the equations is performed with the Cast3M code [12].

3. Results and discussion

We use two methods to compute the magnetic flux density vector : one by using Ampere's

law (10), and the other by using a complete magnetostatic problem (9).

First, temperature and azimuthal **B** field profiles in the whole domain are presented in figures 4 and 5 for three current intensity values: 100, 125, and 150 A, and the two magnetostatic computational formulations. Second, the figure 6 shows the velocity evolution along the axial axis from the cathode tip with these two magnetostatic models and these three current intensities. As we can foresee, higher current intensities lead to higher values for all variables. Moreover, when we use the Ampere's law by neglecting the radial current density, the values of the variables are under-evaluated.

For instance, for 150 A, the maximal temperature, magnetic induction, and velocity are respectively 17303 K, $4.39 \cdot 10^{-2}$ T, 194 m/s when solving a complete magnetostatic problem. On the other hand, when using Ampere's law (10), these values are smaller with 16934 K for the maximal temperature, $3.16 \cdot 10^{-2}$ T for the maximal magnetic flux density vector, and 178 m/s for the maximal velocity.

Therefore, as we can see on the figures 4 and 5, results are slightly changed when choosing a different formulation, but sufficiently important to change the heat and mass transfers in the whole domain. This conclusion is ensured if we calculate the error in the whole domain between the two formulations (LSFEM : full magnetostatic problem, Ampere : Ampere's law according to the equation (10)). These errors are calculated for a X variable according to the following equation : $\left(\frac{\| X_{LSFEM} - X_{Ampere} \|}{\| X_{LSFEM} \|} \right)$. Thus, for 150 A, the differences in the temperature, **B** field, and velocity distributions are respectively 3.5 %, 9.2 %, and 7.7 %. It should be noticed that these error values keep almost unchanged when using 100 or 125 A. The major impact is on the azimuthal **B** field profiles, and hence due to Lorentz forces, on the velocity values. So, as we can remark on figure 6, the formulation choice is significant on the velocity profiles.

4. Conclusion

A two-dimensional axisymmetric unified arc model (cathode, arc, and anode) has been developed. It can predict temperature, current density vector, magnetic field, and fluid flow distributions in the cathode, arc and workpiece domains. The use of the LSFEM method to efficiently compute the magnetic flux density vector has been the innovative part of our work (1 min. per iteration for a 2x1.83GHz CPU with 2Gb). It allowed us not to make a commonly used oversimplification by authors when solving the Ampere's law by assuming the current is almost represented by the axial current density component.

Indeed, numerical simulations showed that using this hypothesis decreases the maximal values of temperature, magnetic field, velocity and mainly changes the magnetic flux density vector and velocity distributions in the whole domain.

Moreover, this LSFEM method gives many benefits because we directly work with **B**, and all the magnetostatic equations are easily solved with a symmetric, positive definite system.

Therefore, the inclusion of the divergence of **B** permits us to extend this model for three-dimensional geometries.

This model is a first step before introducing more physical phenomena by modelling metal vapors, weld pool phenomena, or a three-dimensional arc.

Aknowledgment

This work is supported by Areva NP and the CEA under the PHD grant of Michel Brochard.

References

[1] Hsu, K.C.: Study of the free-burning high-intensity argon arc, Journal of Applied Physics,, 1983, 54, 1293-1301

[2] Gonzalez, J.J.: A numerical modelling of an electric arc and its interaction with the anode: Part II. The three-dimensional model - influence of external forces on the arc column, Journal of Physics D: Applied Physics, 2004, 37, 883-897

[3] Sansonnens, L.H.: Prediction of properties of free burning arcs including effects of ambipolar diffusion, Journal of Physics D: Applied Physics, 2000, 33, 148-157

[4] Debroy, T.: Mathematical modelling of weld phenomena, Journal of Fluid Mechanics, 2001, 6, 21-42

[5] Tanaka, M.: Numerical study of gas tungsten arc plasma with anode melting, Plasma Chem. and Plasma Process, 23 n°3, 2002, 381-389

[6] Hirata, Y.: Numerical model of arc plasma with metal transfer in argon gas shielded metal arc welding, IIW Doc.212-1076-05, Annual IIW assembly, Prague, 2005

[7] Fauchais, P.: Thermal plasmas: fundamentals and applications, vol. 1, Plenum Press, 1994

[8] Ramirez, M.A.: A comparison between two different numerical formulations of welding arc simulation, Modelling Simul. Mat. Sci. Eng., 2003, 11, 675-695

[9] Guermond, J.L.: Éléments finis: Théorie, Applications, Mise en oeuvre, Springer, 2002

[10] Jiang, B.: The Least Square Finite Element Method, Springer, 1998

[11] Metals Handbook: vol. 2, properties and selection: non ferrous alloys and special-purpose materials, American Society for Metals, 1990

[12] Cast3M site, www-cast3m.cea.fr

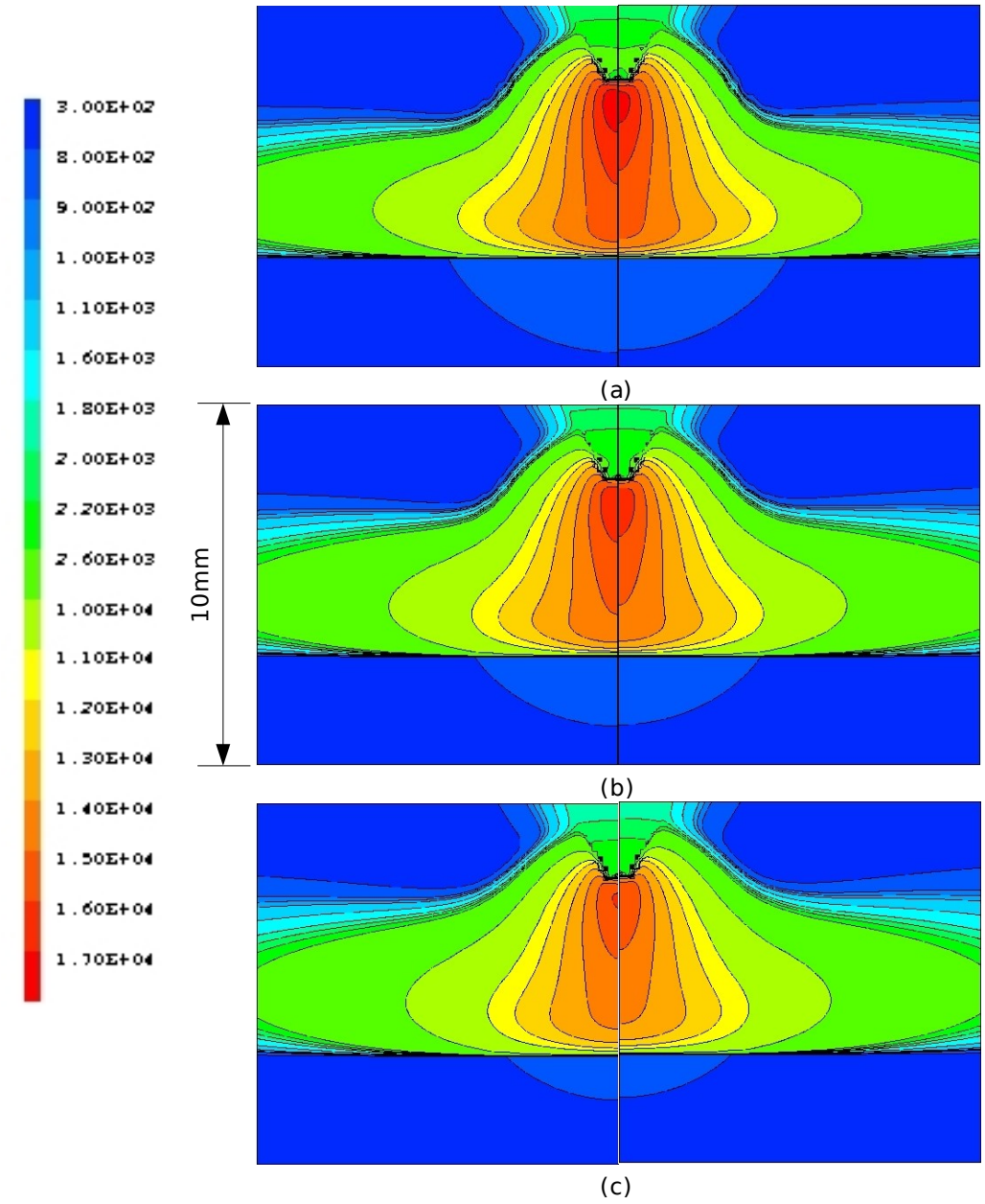

Figure 4 : Isotherms (K) in the cathode, anode, and arc plasma for : (a) 150 A, (b) 125 A, (c) 100 A

Left: full magnetostatic problem; Right: use of Ampere's law with Jr=0

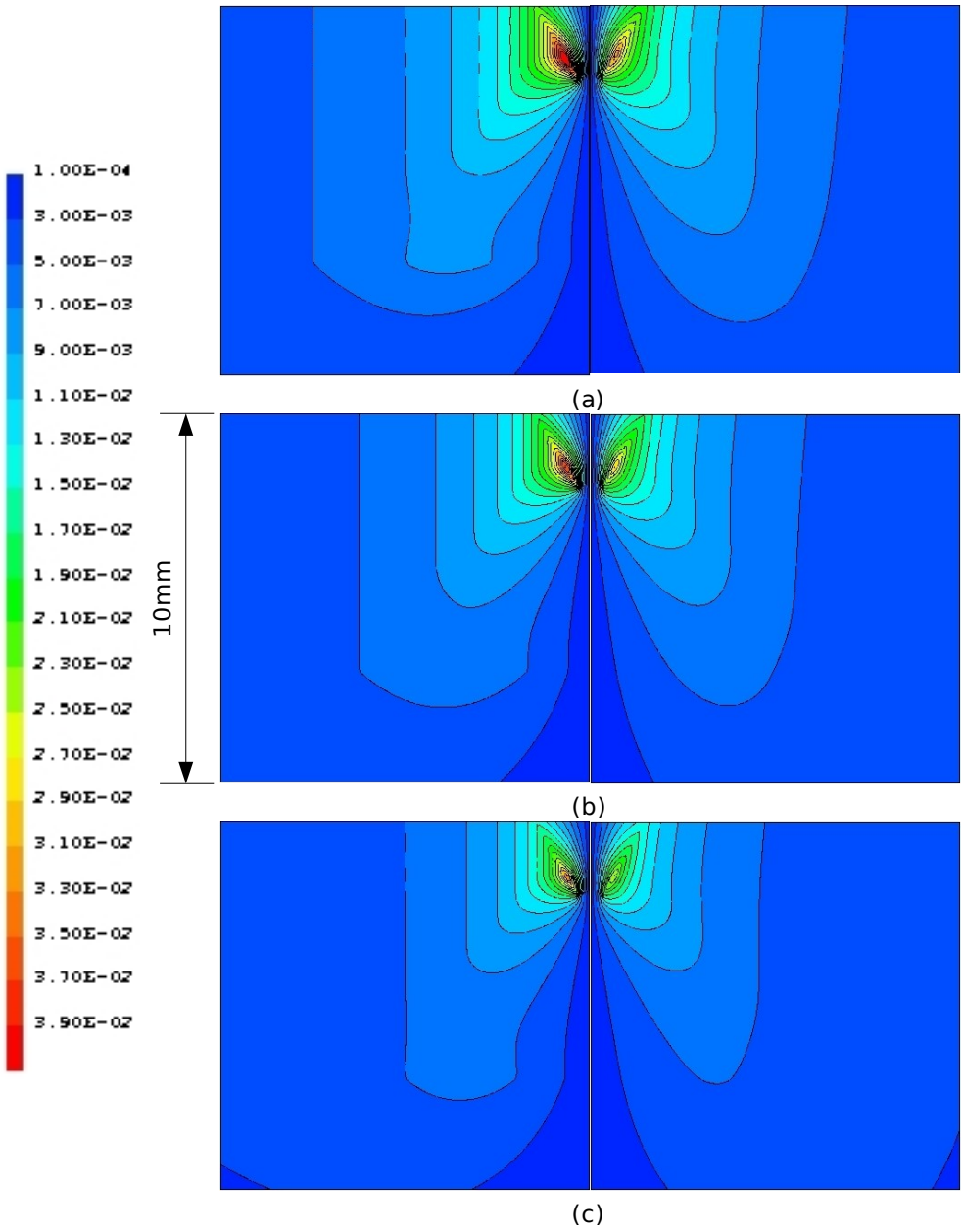

Figure 5 : Azimuthal magnetic field (T) profiles in the cathode, anode, and arc plasma for : (a) 150 A, (b) 125 A, (c) 100 A

Left: full magnetostatic problem; Right: use of Ampere's law with Jr=0

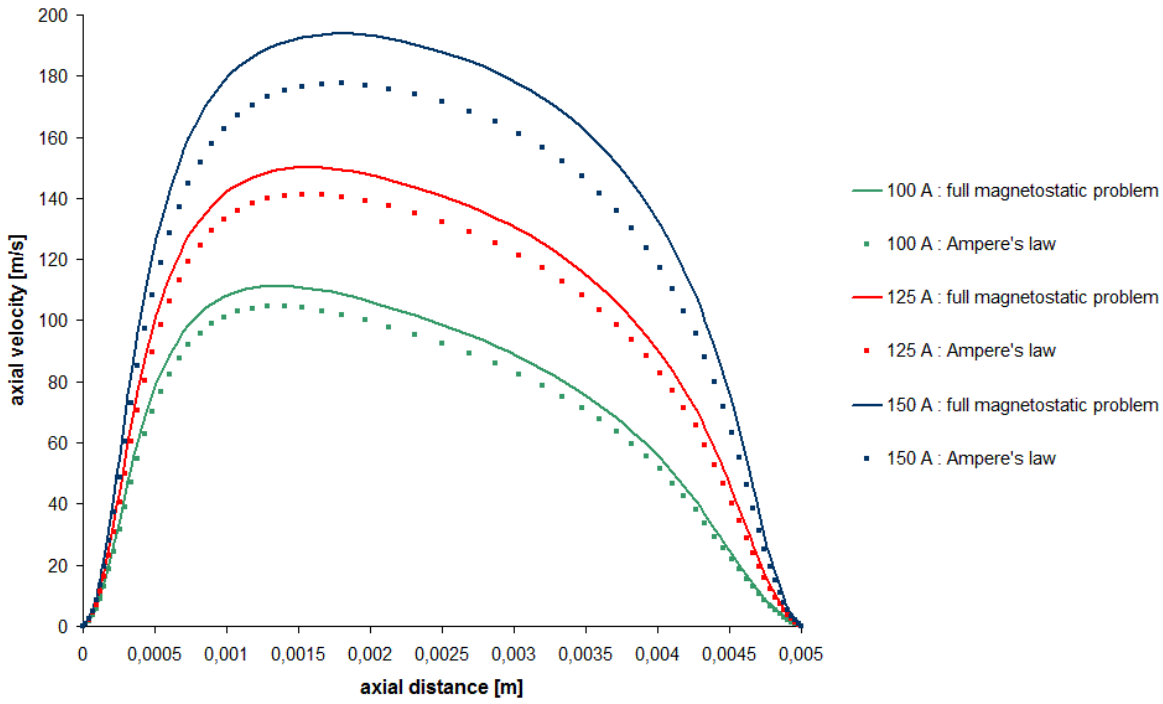

Figure 6 : Axial velocity evolution ($m.s^{-1}$) along the axial axis from the cathode tip to the anode